Hindawi
Advances in Civil Engineering
Volume 2020, Article ID 1725210, 14 pages
https://doi.org/10.1155/2020/1725210

Research Article

Segment Stress Characteristics and Ground Deformation Caused by Constructing Closely Spaced Parallel Tunnels under a Complex Geological Condition

Jianbing Lv,[1] Zikun Li,[1] Xiaodong Xie,[1] Bing Fu,[1] Helin Fu,[2] Hui Zhao,[3] Xulong Li,[4] Zhanrong Li,[5] and Yong Tang[5]

[1]*School of Civil and Transportation Engineering, Guangdong University of Technology, Guangzhou 510006, China*
[2]*School of Civil Engineering, Central South University, Changsha 410012, China*
[3]*School of Foreign Trade and Languages, Guangdong Polytechnic of Science and Trade, Guangzhou 510430, China*
[4]*Shenzhen Transportation Design & Research Institute Co., Ltd., Guangdong, Shenzhen 518003, China*
[5]*China Tunnel Construction Co., Ltd., Guangdong, Guangzhou 510000, China*

Correspondence should be addressed to Helin Fu; 517336864@qq.com

Received 27 October 2019; Revised 7 October 2020; Accepted 30 November 2020; Published 14 December 2020

Academic Editor: Chunshun Zhang

Ground deformation and additional stress on the segments of the firstly constructed tunnel may change significantly due to the construction of another tunnel, which is closely spaced with the existing one. A poor geotechnical condition possibly leads to the interaction between such closely spaced tunnels even making it harder to build such tunnels. A practical project located in Guangzhou City, China, consists of such two parallel tunnels with the smallest distance of 2.6 m, which sat on an upper-soft and lower-hard stratum. A 3D finite element model has been proposed to numerically investigate the behavior of these two parallel tunnels. The numerical results predicted by the FE model are in close agreement with that obtained from the field monitoring system, indicating the accuracy of the proposed FE model. The FE model was then used to further analyze the effect of reinforcing piles in eliminating the detrimental effect on both ground deformation and additional stress of the segments of the existing tunnel as a result of the construction of the new parallel tunnel. The research results obtained from the present paper can provide technical support and guidance for urban subway construction.

1. Introduction

In recent years, the scale of urban underground space development and utilization has been expanding at a fast rate [1], and more and more means have been used to study underground space [2–4]. Parallel shield tunnels with a small space have been often encountered when constructing urban metros in China [5–7]. In such a case, the interaction between the two parallel tunnels becomes significant, leading to the large deformation of surrounding rock and a complex stress state of segments of the lining structure. Therefore, it becomes important to seek an appropriate construction method for such a parallel shield tunnel to ensure the safety of the construction process [8, 9]. In order to enhance the understanding of the interaction between two parallel tunnels, a number of investigations have been conducted including theoretical analysis, numerical simulation, model test, and construction monitoring [10–14]. Fu et al. [15] studied the ground deformation caused by the excavation of double parallel tunnels, in which complex variable theory was employed. The results showed that the superposition principle can be used to determine the ground deformation caused by constructing two closely spaced parallel tunnels. Lei et al. [16] investigated the surrounding rock of shallow bias tunnel with a small spacing under asymmetric loading using theoretical methods, in which the failure mechanism and load characteristics of the surrounding rock of shallow and deep shallow bias tunnel with a small spacing were

presented and analyzed in detail. Zhang et al. [17] used the limit analysis of nonlinear failure criterion and reliability theory to obtain the effect of the clear spacing on the safety levels of the closely spaced parallel tunnels, which provided a theoretical basis to ensure the safety for excavating such closely spaced parallel tunnels. Fang and He [18] concluded that the bending moment of each section in the segment ring of the existing tunnel decreases while the axial force increases due to the construction of the later tunnel, which is parallel to the existing one with a small distance. A real-time data analysis was carried out by Chen et al. [19] to investigate the behavior of two parallel tunnels with a clear spacing of 5.2 m in Shanghai. The analysis results showed that the transverse displacement of the first segment of the second tunnel reaches 13 mm. A finite element model was developed by Lu et al. [20] and the numerical predictions were in good agreement with the monitoring results. It was concluded in their study that that grouting in the tunnel can greatly reduce the influence of the back-going tunnel on the front-going tunnel.

In the coastal cities of China, such as Guangzhou, Shenzhen, and Fuzhou, multilayered geological conditions, which have upper-soft and lower-hard strata, have been often encountered. The mechanical properties of such a geological condition are shown to be apparently different from those of rock and soil conditions. When shield tunneling in such complex strata, it tends to over excavate the upper-soft soils, leading to a significant disturbance to the stratum. As a result, it is difficult for the upper-soft soil to form a stable pressure arising from the arch effect [21], thus causing the detrimental movement of the excavation surface and possible collapse of the soil in the soft soil stratum. The above situation may even lead to large-scale ground subsidence, which brings great challenges to shield tunnel construction [22–24]. It is therefore of great significance to study the effect of a small distance and composite geological condition on the safety of the construction of two closely spaced parallel tunnels. Taking two practical cases located in Guangzhou City as examples, this paper presents a three-dimensional FE model to predict the ground deformation and structural response of the shield liner, which are then compared with the data obtained from the monitor system. The effect of isolation piles on construction safety has been analyzed using the proposed FE model as well.

2. Description of the Practical Cases

2.1. General Information. The two terminals of Tongdewei-Shangbu Station of Guangzhou Metro Line 8 are located at Z (Y) DK21 + 078.150 and Z (Y) DK21 + 694.400, leading to total lengths of the left and right lines of 617.142 m and 616.385 m, respectively. The minimum spacing between these two parallel tunnels is 2.6 m, which is located between ZDK21 + 279 and ZDK21 + 360 and falls in the range of closely spaced parallel tunnels. The right line is designed to be constructed first and then the left line. Both tunnels are designed to be constructed using the Hairike Mud Water Balance Shield Machine with a cutter head diameter of 6280 mm. The inner diameter of the tunnel is 5400 mm. Each segment has a thickness and a width of 300 mm and 150 mm, respectively. Shield tunneling is used in this section.

2.2. Site Conditions. Based on the borehole data, the rock and soil layers along the line are divided into four categories, which are artificial filled soil layer, alluvial-diluvial layer, eluvium, and rock weathering zone. In this area, the hard rock surface immensely fluctuates, and the soft strata above the rock surface are thick. The main soil and rock layers in the small spacing section of the shield are <1> miscellaneous fill, <4–2> mucky soil, <3–1> fine sand, <3-2> medium coarse sand, <3-3> gravel sand, and <9C-2> slightly weathered limestone. Most of the tunnel bodies are located in VI grade surrounding rock, and the surrounding tunnel bodies are mostly sandy layer. Part of the tunnel appears in slightly weathered limestone which has high strength. During shield construction, the proportion of hard rock in the tunnel face is between 0 and 1. The geologic section of the right tunnel is shown in Figure 1.

The depth of the groundwater between the Tongdewei Station and the Shangbu Station is 2.1–5.1 m, and the changes in the groundwater level are dependent on various factors including topography and groundwater recharge sources.

2.3. Difficulties of the Project and Relevant Measures

(1) Diversity of strata: There are not only all soft rock (sand layer) strata but also all hard rock (slightly weathered limestone) strata in test sites. There are also upper-soft soils, below which there are hard strata with different composite ratios of hard and soft rocks. The diversity of strata leads to complicated control of tunneling parameters.

(2) The effect of the tunneling process of the left line on the right tunnel is a complicated extrusion and unloading process, and the extrusion is mainly caused by the diffusion of the cutterhead pressure and the grouting pressure of the shield tail in the formation. The reinforcement measures for the right tunnel and the timing and location of installing the reinforcement must be decided on a rational basis.

(3) The left tunnel is only 2.6 m away from the right tunnel in the small spacing interval. Hence, the construction of the left tunnel increases the disturbance to the surrounding strata and existing tunnels. Especially in the upper-soft and lower-hard composite strata, construction easily leads to over-excavation of shielding excavation at the upper-soft soils, resulting in greater uneven settlement. The engineering problems are how to control the surface settlement during the construction of the left tunnel and to ensure the safety of the existing tunnel on the right side.

(4) The small-pitch tunnel uses 800 mm diameter isolated bored piles spacing at 1000 mm as reinforcement. The base of the bored pile is either 1 m into the

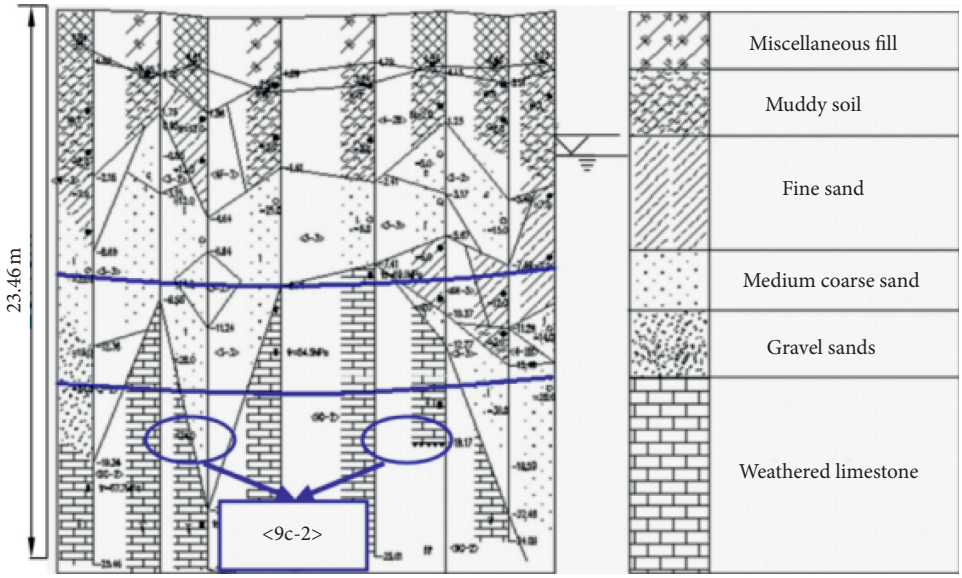

Figure 1: Geological profile map.

arch of the shield tunnel or 1 m into the micro-weathered limestone formation. The bored piles have been arranged from the archtop 3 m to the lower reinforced bars, and the rest are C30 plain concretes.

2.4. Reinforcement Scheme of Small Spacing Tunnel. To reduce the influence of the right tunnel and ensure the safety of the tunnel structure, it is necessary to isolate and protect the tunnels with small spacing by bored piles. In the Z (Y) DK21 + 279~Z (Y) DK 21 + 360 range, a row of 800 mm@ 1000 mm bored piles is constructed to isolate these two closely spaced parallel tunnels. The location of the isolation pile is shown in Figure 2. From Pile 80 to Pile 124, the total number of isolation piles is 45. Among them, in the range of ZDK21 + 319.034~ZDK21 + 329.134 mileage, a total of 10.1 m has been carried out in the connecting passage stratum, which has been strengthened by outer diaphragm wall + internal rotary jet grouting pile. The strengthening body can satisfy the requirements of tunnels under construction as well as in service; therefore, the isolation pile has not been used in this area. The diameter of the pile is 800 mm and the thickness of the protective layer is 70 mm. The concrete of the bored pile is C30 underwater concrete, and the steel bars are HPB300 and HRB400. Among them, because the project is located in the karst area, the strata fluctuate greatly, providing input conditions for the construction of isolation piles to prove the strata, ZDK21 + 279.000~ZDK21 + 360.000 mileage range every two piles to drill a geological advanced drilling. According to the results of geological advance drilling, the scope of construction of isolation piles is determined. If the stratum below the arch waist is <9C-2> stratum, small interval tunnel treatment will not be needed; otherwise, the isolation of 800 mm@1000 mm bored piles will be needed; the bottom of bored piles enters 1.0 m below the arch bottom of shield tunnel or 1 m into <9C-2> stratum, the reinforcement is distributed in the range of bored piles below 3 m above the arch top, and the remaining sections are C30 plain concrete. Figures 2 and 3 are planar and sectional diagrams of isolation pile reinforcement.

3. Monitoring and Analysis of Surface Settlement in Right Shield Tunnel Construction

3.1. Definition of Hard Rock Height Ratio. The foundation of the north extension part of Guangzhou Metro Line 8 is composed of upper-soft and lower-hard strata. The properties of the overlying soil layer of the shield tunnel are close to that of the whole metro line. However, the properties of the hard rock are shown to be varied along the tunnel, leading to different hard rock proportions at different excavation faces. In order to minimize the stratum disturbance induced by the left shield construction, the influence of the different proportion of hard rock in the right shield excavation face on stratum deformation is first investigated, which provides corresponding useful information to ensure safety during the construction process of the later shield line. Hard rock height ratio is proposed and defined as the ratio of hard rock height to total height in shield excavation face:

$$\beta = \frac{h}{D}, \tag{1}$$

where β is the ratio of hard rock height to total height in shield excavation face, h is the height of soft rock, and D is the total height of the tunnel excavation face, as shown in Figure 4.

3.2. Layout of Settlement Monitoring Points. On the basis of fully considering the surrounding environment grade and the operability of monitoring implementation in Tongdewei-Shangbu Station, ground settlement monitoring in

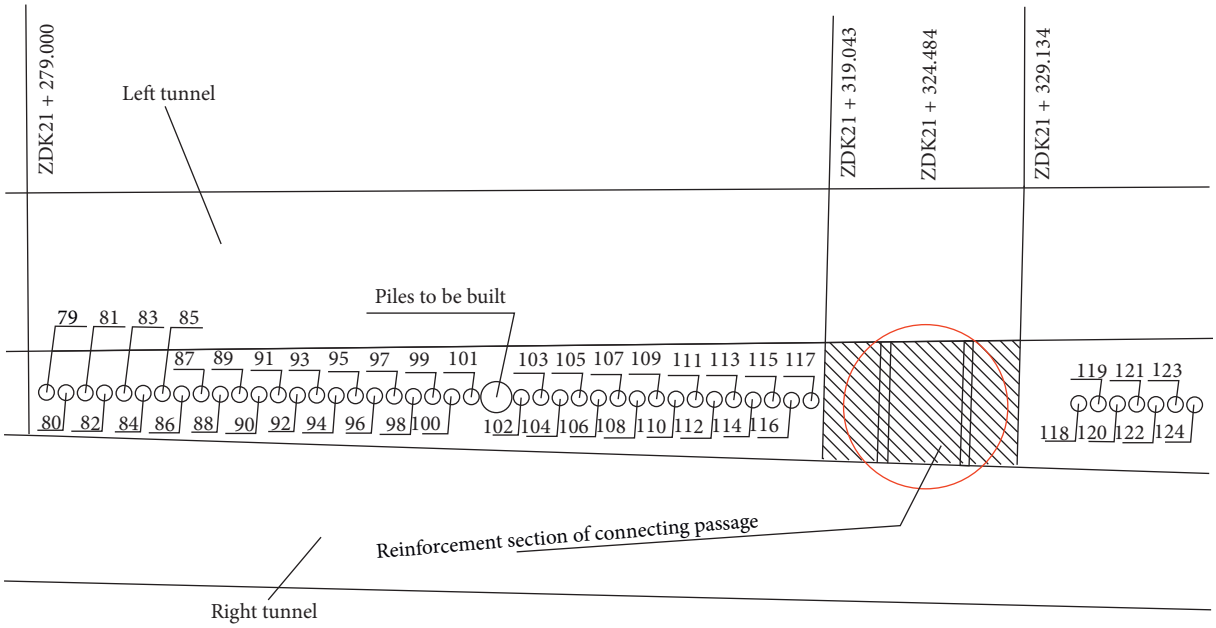

Figure 2: Plan view of isolation pile reinforcement.

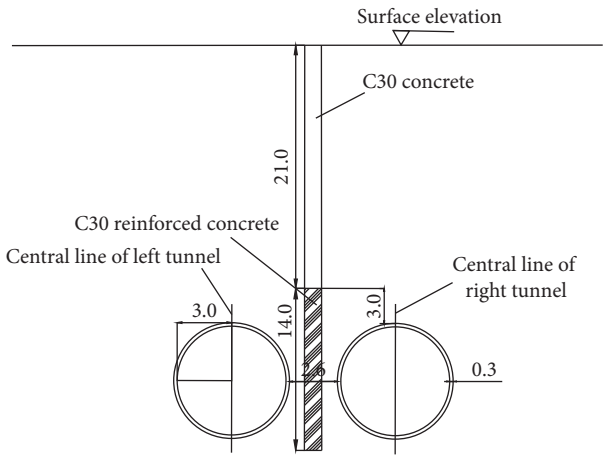

Figure 3: Profile of isolation pile reinforcements.

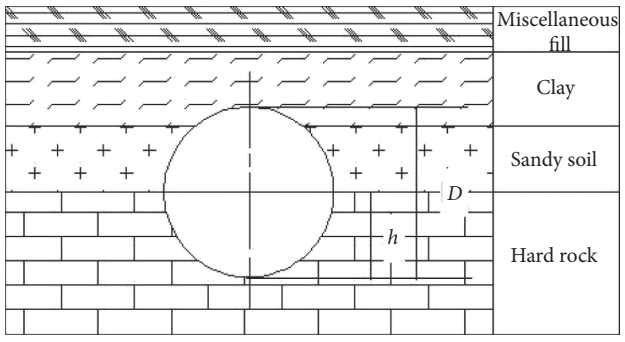

Figure 4: Composite stratum sketch map of shield tunneling interval at Tongdewei-Shangbu Station.

shield tunneling interval can be divided into longitudinal monitoring and transverse monitoring. Longitudinal monitoring points are installed every 5 m along the tunnel alignment. Transverse monitoring is distributed from the center of the shield vault to both sides, from near to far, and increases by 3–5 m between the measuring points. The detailed layout is shown in Figures 5 and 6.

3.3. Monitoring and Analysis of Surface Settlement. In order to determine the relationship between the hard rock height ratio occupied by excavation face and surface settlement, five sections with different hard rock height ratios in the right tunnel are selected out for monitoring based on the results of the geotechnical investigation report and field investigation. The surface monitoring points above the tunnel vault are YD170, YD203, YD200, YD161, and YD162. The hard rock height ratios to the tunnel section are 0, 0.20, 0.50, 0.85, and 1.00, respectively. The variation rules of surface transverse and longitudinal settlements under the same shield tunneling measures are obtained according to the statistical analysis of the actual monitoring data of these monitoring sections.

3.3.1. Monitoring Results of Transverse Subsidence of Ground Surface. Figure 7 shows the transverse subsidence of the ground surface. The curve is a transverse surface settlement map of the monitoring section perpendicular to the vault of the shield tunnel. In shield tunneling, the transverse surface settlement law of the five monitoring sections shows that the corresponding surface settlement value of the tunnel vault is the largest, and the settlement value gradually decreases with the transverse monitoring point away from the vault of the

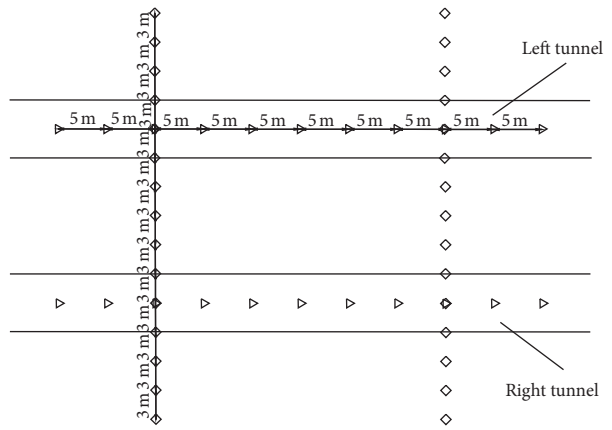

Figure 5: Longitudinal layout of ground subsidence monitoring points.

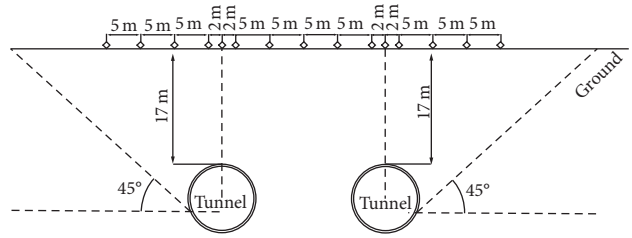

Figure 6: Transverse layout of ground subsidence monitoring points.

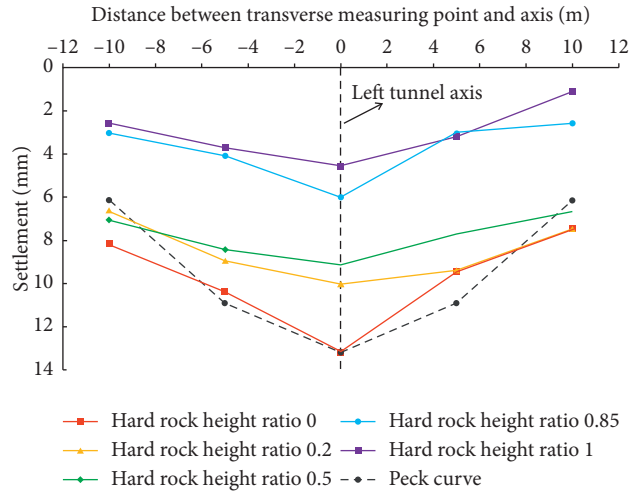

Figure 7: Transverse surface settlement curves of different hard rock height ratios.

tunnel. The settlement value near the monitoring point of the tunnel vault changes faster than that far from the monitoring point of the tunnel vault. Generally, the measured transverse surface subsidence curve has an evident settlement trough, which is consistent with the predicted curve of Peck.

Transverse surface subsidence is affected by the hard rock height ratio. The general trend is that the value of surface subsidence correspondingly decreases and settlement trough becomes shallow with the increase in hard rock height ratio. The surface settlement above and near the tunnel vault is affected by the hard rock height ratio. The settlement values of monitoring points far from the tunnel vault are close when the hard rock height ratios are 0–0.5 and 0.85–1, except for the depth of the settlement trough. The settlement value reaches a maximum value of 13.2 mm when the hard rock height ratio is 0.

3.3.2. Monitoring Results of Longitudinal Subsidence of Ground Surface. Figure 8 shows the curves of the surface subsidence, which is the surface subsidence under different

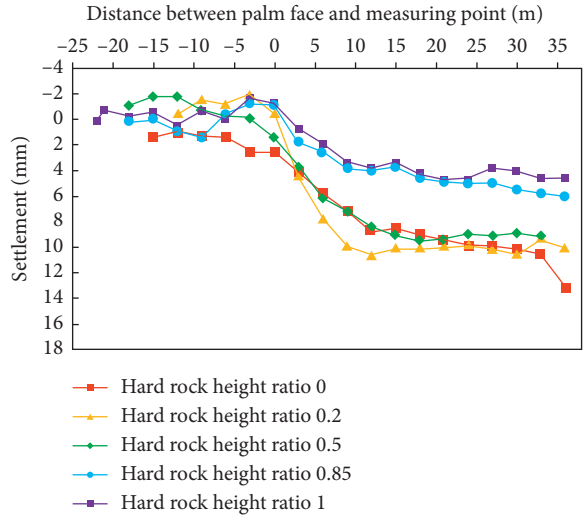

Figure 8: Longitudinal surface subsidence curves of different hard rock height ratios.

hard rock height ratios during the shield tunneling. From the figure, obvious uplift is observed on the surface at approximately 15–20 m ahead of the excavation face due to the influence of tunneling pressure on the excavation face, which belongs to negative stratum loss. At approximately 5 m ahead of the excavation face, surface deformation changes from uplift to subsidence with an accelerating trend, and surface deformation is the settlement deformation under the influence of shield structure gaps. At the area of 5–10 m behind the excavation face, the surface settlement varies greatly, with the maximum difference of settlement value up to 2.8 mm. This subsidence belongs to normal stratum loss. At approximately 20 m behind the excavation face, the surface settlement is no longer affected by shield tunneling. Longitudinal surface subsidence is significantly affected by the hard rock height ratio, which shows that surface subsidence decreases with the increase in hard rock height ratio. The surface longitudinal subsidence curves of tunnels with different hard rock height ratios are compared. The results show that, with the increase of the hard rock height ratio, the location of surface deformation begins to decrease from approximately 15 m ahead of the excavation face to approximately 10 m. Moreover, the surface subsidence rate after the excavation face has a decreasing trend with the increase in hard rock height ratio. Generally, the influence degree and scope of shield tunneling on surface longitudinal settlement decrease with the increase in hard rock height ratio.

Through the above research, special attention should be paid to the construction in the area of 0–0.2 and 0.5–1 hard rock height ratio, so as to prevent the uneven settlement of the surface caused by the construction in the area of sensitive hard rock height ratio.

4. Numerical Investigation

4.1. Proposed Finite Element Model. A three-dimensional finite element model was developed by using Midas/GTS. The part within 6 times the radius of the tunnel is meshed in this model according to the geomechanical theory of [25]. Therefore, the proposed FE model is 60 m in the radial direction, 72 m in the longitudinal direction, and 38 m in the vertical direction. The overlying soil layer of the tunnel is 14 m high and the distance between the outer edges of the two tunnels is 2.6 m. The hybrid mesh of tetrahedron and hexahedron with high accuracy is adopted in the mesh. The soil layer is simulated by solid element. Shield shell, segment, and grouting layer are simulated by plate element, and bored isolation cast-in-place pile is modeled using beam elements. According to the Code for Design of Concrete Structures, the elastic modulus of segments should be 34.5 GPa. Considering the effect of annular and longitudinal splicing on the stiffness reduction of segments, the elastic modulus of segments should be reduced by 80% of the recommended value in the code, that is, 27.6 GPa. Poisson's ratio of the segment is 0.2. The segment grouting layer is equivalent to the slurry equivalent layer [26], and the thickness of the equivalent layer is 0.3. The calculating process does not consider the hardening process of the slurry [27]. In addition to the free boundary in the Z direction, the lower boundary and the surrounding boundary are constrained by fixed constraints. The modified Mohr-Coulomb failure criterion is adopted in geotechnical constitutive law. It can be seen from the surface subsidence law corresponding to different hard rock height ratios that when the hard rock height ratio is 0, the surface subsidence has the greatest impact, so the hard rock height ratio in the numerical model is set to 0, of which the tunnels are excavated in the stratum above the limestone. Through the above modeling process, the finite element analysis model is divided into 75127 nodes and 145513 elements, as shown in Figure 9. The physical and mechanical parameters of the model are shown in Table 1.

4.2. Simulation of Working Conditions. The simulation does not consider the scope of the connected aisle, because the connected aisle is built in the range of ZDK21 + 319.034~ZDK21 + 329.134 mileage, and the

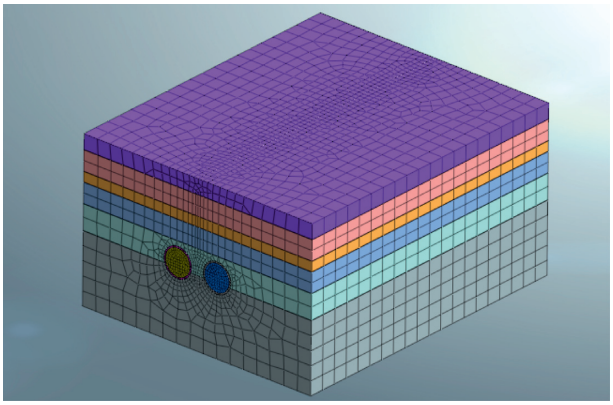

Figure 9: Finite element model.

Table 1: Geotechnical physical and mechanical parameters.

Soil name	Severe γ (kN/m^3)	Deformation modulus E0 (MPa)	Cohesive force C (kPa)	Internal friction angle ϕ (°)	Poisson's ratio (μ)
Miscellaneous fill	16.5	2.5	8	10	0.35
Mucky soil	17	5	12.6	12.8	0.3
Fine sand	20.3	12	15	35	0.3
Medium coarse sand	19.6	40	10	30.5	0.3
Gravel sand	20.8	50	10	30.5	0.3
Slightly weathered limestone	24.5	10000	1500	55	0.3

reinforcement of the connected aisle fulfills a request. In order to accurately simulate the influence of shield induced on stratum and structure, the following factors are considered: shield thrust pressure of 0.25 MPa and grouting pressure of 0.36 MPa. The distribution of the stress field is analyzed prior to the excavation process. In order to improve the efficiency of calculation and analysis, the length of four segments is taken as a construction step in each excavation, while shield shell elements and tunnel face pressure are activated to stabilize the excavation surface. During the next construction step, the segment elements and grouting pressure at the position of the previous construction step are activated. This will continue to circulate until the construction of the two tunnels is completed. There are 24 construction steps in the excavation of both left and right lines. In order to accurately reflect the effect of the left shield construction on the right tunnel, the displacement field should be cleared after the completion of the right tunnel excavation. The stress field and displacement field of the subsequent excavation are incremental values caused by the excavation of the left tunnel.

In this paper, combined with the design of an isolation pile reinforcement scheme, the following two working conditions are selected in the numerical simulation, and the effect of double-line shield construction is analyzed.

Working condition 1: the horizontal spacing between these two tunnels is 2.6 m without reinforcing measures.

Working condition 2: the horizontal spacing between the two tunnels is 2.6 m with 800 mm diameter bored cast-in-place piles as reinforcements.

4.3. Surface Settlement and Horizontal Displacement. The vertical displacement nephogram of the stratum before and after model reinforcement is given in Figure 10. The surface corresponding to the 10th ring of the model is selected for observation and analysis, and the corresponding transverse settlement curve is drawn, as shown in Figure 11. Due to the continuous construction process of the two tunnels, the ground surface has undergone two types of continuous subsidence. In general, the settlement curve of double-line construction varies with the variation of tunnel spacing. That is to say, when the spacing between these two tunnels increases, the surface settlement curve changes from *W*-type distribution to *V*-type distribution. In case of no reinforcement, the settlement curve after the completion of double-line construction is shown to be a typical Peck curve distribution, that is, "*V*" distribution. The subsequent digging tunnel has a significant effect on the disturbance of surrounding rock. The maximum settlement occurs at the midpoint of the center of the two tunnels with a value of −17.4 mm. After reinforcing with isolation piles, the surface settlement curve became *W*-shaped, and the maximum settlement value occurs near the center of the two tunnels but significantly decreased to −10 mm. From the graph, it can be seen that the maximum value of the surface settlement curve is reduced by about 7.4 mm after the reinforcement of isolation piles, and the settlement curve is changed from "*V*" type to "*W*" type. This indicates that the use of isolation piles led to the distance between tunnels "larger" and significant decrease in the surface settlement of these closely spaced parallel tunnels.

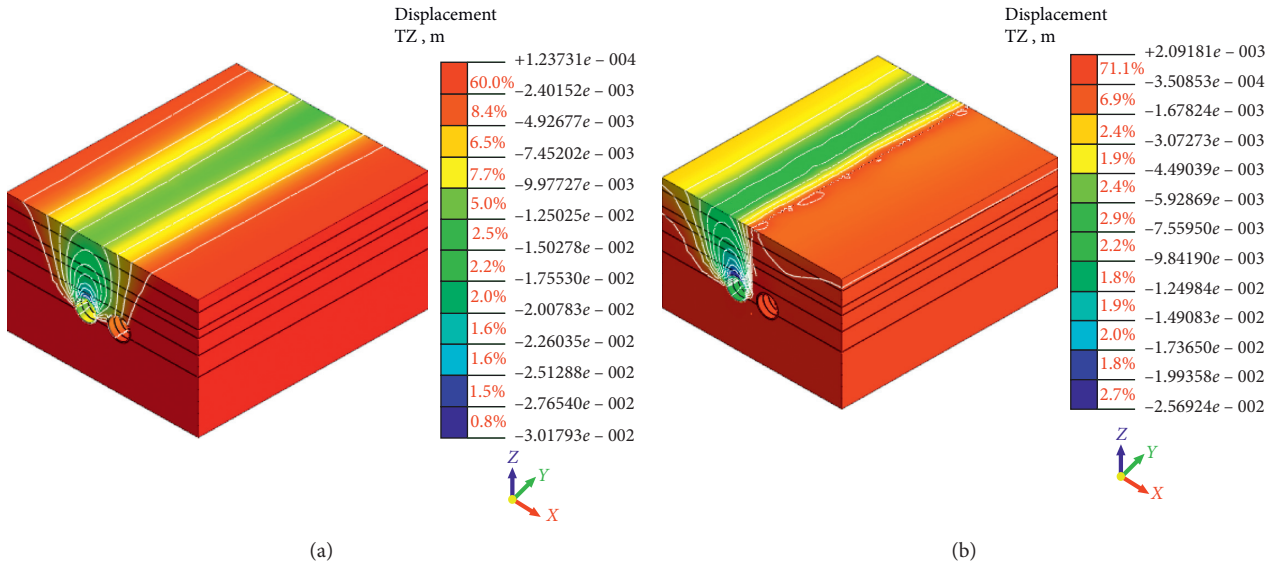

Figure 10: Stratum settlement nephogram before and after reinforcement. (a) Nephogram of unreinforced stratum settlement; (b) nephogram of stratum settlement after reinforcement.

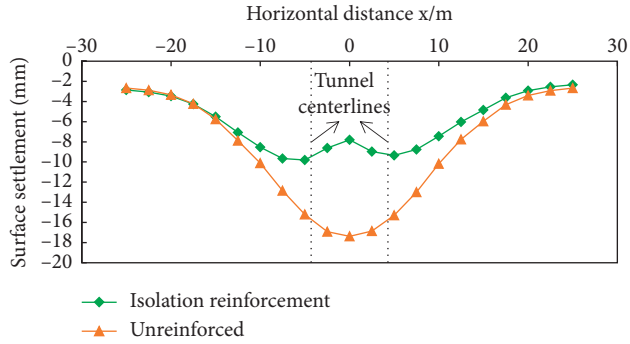

Figure 11: Transverse subsidence curve of the surface before and after reinforcement.

The horizontal displacement nephograms of stratum with and without reinforcing measures are shown in Figure 12. The surface corresponding to the 10th ring of the model is selected for observation and analysis, and the corresponding horizontal displacement curve is drawn, as shown in Figure 13. It can be seen from the figure that the horizontal displacement curves of the surface before and after the reinforcement are symmetrical concerning the central position of the two tunnels. The maximum horizontal displacement of the surface is 9.1 mm when it is not reinforced, which is located at about 10 meters in the center of the two tunnels. With isolation reinforcing piles, the maximum horizontal displacement of the ground surface decreases to 6.7 mm, which is approximately 13 m in the center of the two tunnels. The numerical results show that the influence of shield tunneling after the isolation pile reinforcement on the horizontal displacement of the stratum is also reduced to a certain extent. In addition, the influence of the reinforcement on the stratum will spread to the outside of the two tunnels, which reduces the stress concentration of the surrounding rock of the middle column with small spacing.

4.4. Deformation of Prior-Dug Tunnel Segments without Reinforcements. The radial deformation of a segment is an important factor to evaluate the safety level of tunnels. In this study, the changes in the diameters of the prior-dug tunnel segment along the lines of AB and CD (Figure 14) have been analyzed using the proposed FE model. Two typical segments of the right line have been selected for detailed investigation. The two selected segments are those at 132nd and 142nd rings, which corresponded to the 10th and 20th rings of the numerical model, respectively, as shown in Figure 14.

Figures 15 and 16 give the variations of the displacements in both horizontal and vertical directions of the right line segment during the excavation process of the left line. Taking the 132nd ring of the right tunnel as an example, the relative deformation of the ring during shield construction is

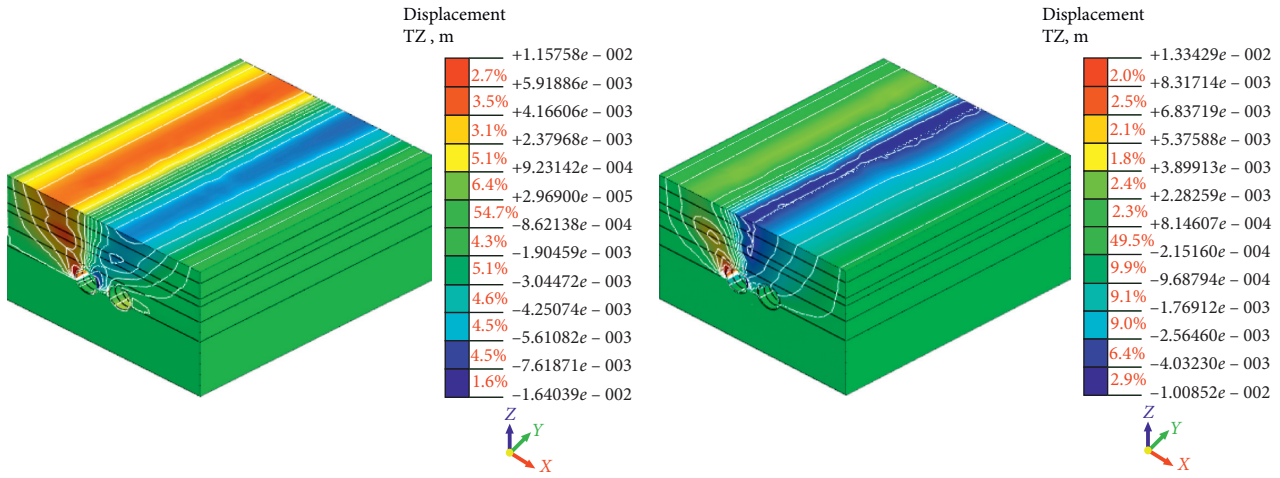

Figure 12: Horizontal displacement nephogram of strata before and after reinforcement. (a) Horizontal displacement nephogram of unconsolidated strata. (b) Horizontal displacement nephogram of consolidated strata.

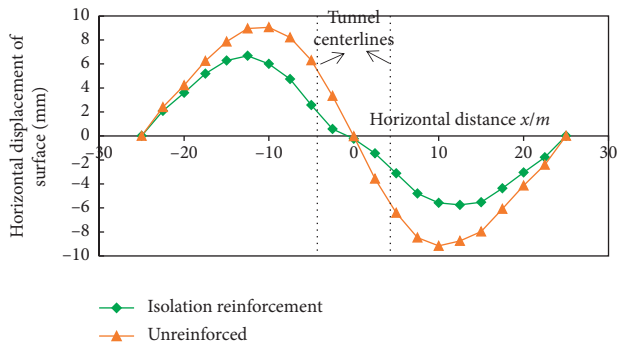

Figure 13: Horizontal displacement curve of the surface before and after reinforcement.

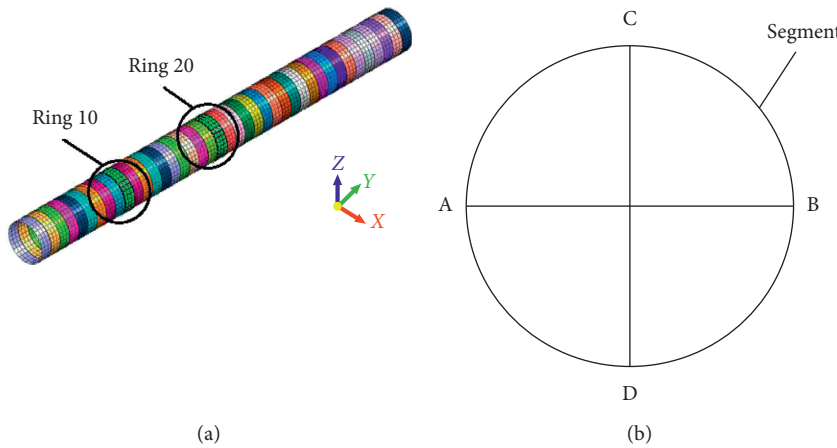

Figure 14: Drawing of prior-dug tunnel segments monitoring. (a) Schematic diagram of prior-dug tunnel segments selection. (b) Diagram of segment monitoring points.

studied. The third construction step is that the left line excavation face is about to reach 132nd ring; after that, the left shield excavation face in the process of passing through the 132nd ring forms the fourth step. The fifth step of construction is presented by passing through the 132nd ring completely of the left shield excavation. As shown in

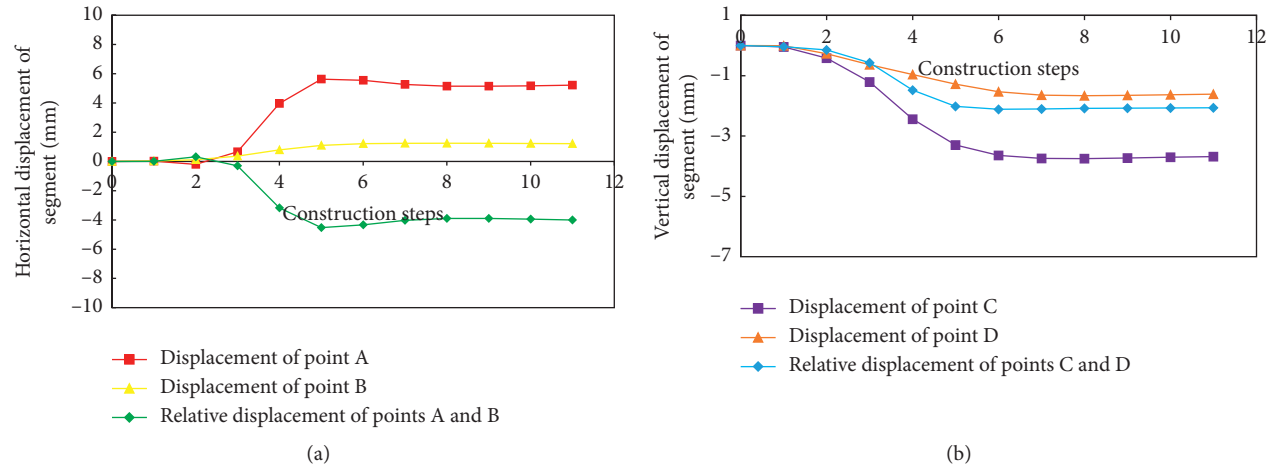

Figure 15: Displacement curve of the 132nd ring segment in the construction processes of left tunnel excavation. (a) Horizontal displacement curves of points A and B. (b) Vertical displacement curve of points C and D.

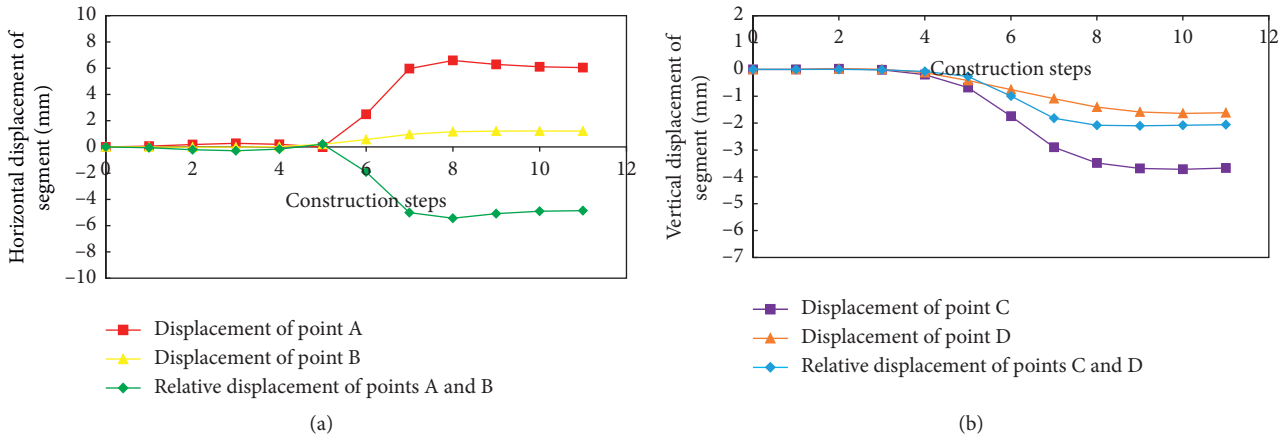

Figure 16: Displacement curve of 142nd ring segment in the construction processes of left tunnel excavation. (a) Horizontal displacement curves of points A and B. (b) Vertical displacement curve of points C and D.

Figure 16, prior to the third construction step, the horizontal displacements of points A and B are small and approximately remain unchanged. At that stage, the vertical displacements of point C and point D are 1.2 mm and 0.6 mm, respectively. When the 132nd ring was passing through (i.e., the fourth step), the horizontal displacement of point A and point B increased dramatically to 4.3 mm and 1.1 mm, respectively, leading to the corresponding relative displacement of −2.4 mm. The vertical displacement of point D increases to −0.9 mm with the corresponding relative displacement being −1.48 mm. It is assumed that the sudden changes in the deformation of the 132nd ring segment are mainly due to the changes in the changed in the grouting pressure and other factors as a result of the passing of the excavation face of the backward shield machine through the monitoring section. When the construction step reaches the 5th construction step, the displacement of the 132nd ring A point reaches the maximum value; that is, the maximum displacement is 5.6 mm. The maximum vertical displacement of point C is −3.75 mm, which occurs in the eighth construction step. Figure 16 illustrates that, after the fifth construction step, the horizontal displacement of points A and B decreases to a certain extent and tends to be stable. The main reason is that the rear shield has a certain unloading rebound effect on the monitoring section after passing through the monitoring section. The rebound value of A point is 0.49 mm. From Figure 16, it can be seen that the deformation of the 142nd ring segment varied in a similar manner.

4.5. Segment Deformation Analysis of Small Spacing Construction with and without Reinforcements. To facilitate the comparative analysis of the effect of the left shield tunnel construction before and after the reinforcement on the right segment, the segment deformation curves of the whole process of shield tunnel construction with and without reinforcement are shown in Figure 17. Due to the page limit of the present paper, only the deformation of the 132nd ring segment of the right line is analyzed. After being reinforced

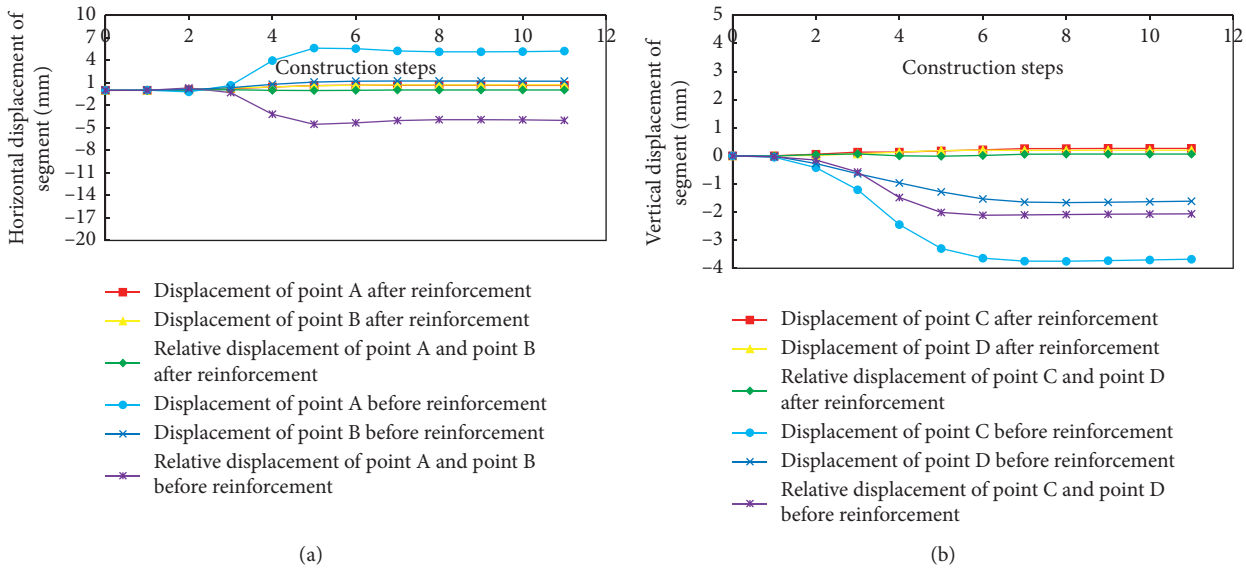

Figure 17: Deformation curve of the right line 132nd ring segment caused by left shield excavation before and after reinforcement. (a) Horizontal displacement curves of points A and B before and after reinforcement. (b) Vertical displacement curve of points C and D before and after reinforcement.

by isolation piles, it can be seen from the figure that the relative displacements of segments, points A, B, C, and D, are greatly reduced. The maximum horizontal displacements of point A and point B are 0.7 mm and 0.8 mm, respectively, and the maximum vertical displacements of C and D points are 0.3 mm and 0.2 mm. The relative displacement of the segments is less than 0.1 mm. The relative value of point A and point B is 4.5 mm for the unreinforced case, and the displacement value of point A is much larger than that of point B, indicating that the segment is "extruded." After reinforcement, the displacement of each measuring point is almost equaled, which shows that the trend of "extrusion" of the preceding segment has been greatly improved.

5. Verification of the Proposed FE Model Using Field Monitoring Results

5.1. Monitoring Method and Layout of Measuring Points for Additional Stress of Segments. The additional stress of the segment caused by the excavation of the left tunnel was measured by a number of strain gauges installed on the target segment of the right line. The strain gauges were installed through a standard procedure, which consisted of steps: (1) preparation of concrete surface to be bonded with strain gauges; (2) application of two-component adhesive to strain gauges; (3) bonding of strain gauges to the prepared concrete surface. After that, the strain gauges were connected by wires to the data logger. In order to ensure that the strain gauges are not affected by external factors, protective stapes were used to cover the strain gauges. At the same time, the lead wire will be led to the trolley to avoid the damage of the wire and sensor by hanging, and at the same time, it is convenient for monitoring. The actual site monitoring arrangement is shown in the following Figure 18.

5.2. Processing Method of Additional Stress Monitoring Data. The static strain monitor is used to automatically collect the additional microstrain of the segment. The acquired microstrain is transformed into strain value, and the additional stress value is obtained by the relationship between stress and strain. The specific transformation is as follows:

$$\varepsilon = 10^{-6}\,\mu\varepsilon,$$
$$\sigma = E\varepsilon. \tag{2}$$

In the formula, $\mu\varepsilon$ is microstrain and dimensionless, which is directly collected by a static strain gauge. ε is the additional strain value and E is the elastic modulus of the segment. The elastic modulus of the C50 segment is 3.45×10^4 MPa. σ is the additional stress of the segment.

5.3. Comparison between Monitoring Results and Numerical Predictions. The additional stress of the segment near the arch waist of the 132nd ring of the right segment is selected for the comparison. Due to the limitation of monitoring conditions, the 132nd ring of the right line can only be monitored when the excavation surface of the left line arrives at the monitoring section. The variation curve of the additional stress of the right segment in the whole process of shield passing through the monitoring plane is shown in Figure 19. Figure 19 demonstrates that the additional stress of the segment increases continuously in the range of 0 to 14 m after the left shield passes through the monitoring plane. The maximum additional stress is −2.2 MPa at 12 m after passing through the right monitoring plane. The main reason is that the cutterhead pressure of the left shield and the grouting pressure of the shield tail have great influences on the right segment. When the distance between the excavation surface and the monitoring surface of the left shield is more than 14 m, the additional stress begins to decrease

(a) (b)

Figure 18: Site monitoring chart. (a) Layout of strain gauges. (b) Data acquisition of static monitor.

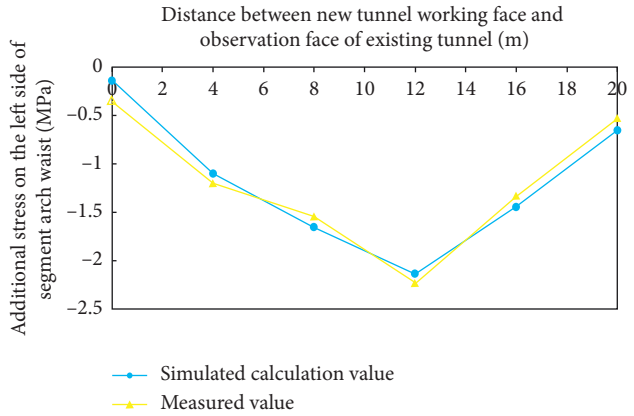

Figure 19: Additional stress of no. 132 ring: monitoring results versus numerical predictions.

gradually. The main reason is that the excavation face of the left shield has an unloading effect on the right segment after passing through the segment at a certain distance.

From Figure 19, it can be seen that the simulated values are close to the measured values, and the trends of the two are consistent, indicating the accuracy of the proposed FE model for predicting the behavior of closely spaced parallel tunnels.

6. Conclusion

The interaction between closely spaced parallel tunnels is significant, which surely results in a large disturbance in the ground surface and significant values of the additional stress of the segments as a result of the construction of the later tunnel. When such closely spaced tunnels rest on poor geotechnical conditions, the analysis of the interaction and corresponding structural response of the segments of the tunnels may become difficult. In the present paper, a 3D FE model has been proposed to analyze the interaction of these two parallel tunnels with and without reinforcing concrete piles, and then the numerical results predicted by the FE model were compared with the monitor results, indicating the accuracy of the FE model. The conclusions can be drawn as follows:

(1) After the completion of the first-constructed tunnel, the surface subsidence has the largest value corresponding to the hard rock ratio of 0, the maximum transverse surface settlement value of the surface is 13.2 mm, and the influence length of the longitudinal settlement is about 35 mm. However, it is necessary to pay special attention to the construction of subsequent digging shield when the hard rock height ratio is in the range of 0–0.2 and 0.5–1 to prevent uneven surface settlement during the construction of the sensitive hard rock height ratio section.

(2) Reinforcing measures with isolation piles can effectively reduce the effect of small spacing shield construction on the deformation of the ground and the prior-dug tunnel segments. After reinforcement, the maximum settlement of the ground surface decreases from 17.4 mm to 10 mm, and the maximum deformation of horizontal displacement decreases from 9.1 mm to 6.7 mm. Before reinforcement, the maximum deformation of the arch waist is 5.6 mm and the maximum convergence

is 4.5 mm. After reinforcement, the displacements of right segments are significantly reduced, and the relative displacement values in horizontal and vertical directions are less than 0.1 mm.

(3) The numerical results predicted by the proposed 3D FE model are in close agreement with the field monitoring results. The additional stress of the segment has the same characteristics as the deformation; that is, the segment is squeezed before the excavation surface passes through the monitoring section, and the segment is unloaded and rebounded after the excavation surface passes a certain distance from the monitored section.

Data Availability

The data used to support the findings of this study are included within the article.

Conflicts of Interest

The authors declare no conflicts of interest.

Acknowledgments

The authors acknowledge the financial support provided by the Guangdong Provincial Natural Science Foundation of China (Grant no.2019A1515011397), and Chinese National Natural Science Foundation (Grant nos. 51978668 and 51978177).

References

[1] C. W. W. Ng, K. Y. Fong, and H. L. Liu, "The effects of existing horseshoe-shaped tunnel sizes on circular crossing tunnel interactions: three-dimensional numerical analyses," *Tunnelling and Underground Space Technology*, vol. 77, pp. 68–79, 2018.

[2] B. X. Yuan, L. Xiong, L. Zhai et al., "Transparent synthetic soil and its application in modeling of soil-structure interaction using optical system," *Frontiers in Earth Science*, vol. 7, p. 276, 2019.

[3] B. Yuan, M. Sun, L. Xiong, Q. Luo, H. Pradhan, and H. Z. Li, "Investigation of 3D deformation of transparent soil around a laterally loaded pile based on a hydraulic gradient model test," *Journal of Building Engineering*, vol. 28, no. 3, p. 101024, 2020.

[4] B. X. Yuan, M. Sun, Y. X. Wang, L. H. Zhai, and Q. Z. Luo, "Full 3D displacement measuring system for 3D displacement field of soil around a laterally loaded pile in transparent soil," *International Journal of Geomechanics*, vol. 19, no. 5, Article ID 04019028, 2019.

[5] M. Zhang and M. Huang, "Geotechnical influence on existing subway tunnels induced by multiline tunneling in shanghai soft soil," *Computers and Geotechnics*, vol. 56, pp. 121–132, 2014.

[6] Q. Liang, J. Li, D. Li, and E. Ou, "Effect of blast-induced vibration from new railway tunnel on existing adjacent railway tunnel in xinjiang, China," *Rock Mechanics and Rock Engineering*, vol. 46, no. 1, pp. 19–39, 2013.

[7] X. Lin, R. Chen, and H. Wu, "Deformation behaviors of existing tunnels caused by shield tunneling undercrossing with oblique angle," *Tunnelling and Underground Space Technology*, vol. 57, pp. 241–256, 2016.

[8] H. Y. Liu, J. C. Small, J. P. Carter, and D. J. Williams, "Effects of tunnelling on existing support systems of perpendicularly crossing tunnels," *Computers and Geotechnics*, vol. 36, no. 5, pp. 880–894, 2009.

[9] T. E. Vorster, A. Klar, K. Soga, and R. J. Mair, "Estimating the effects of tunneling on existing pipelines," *Journal of Geotechnical and Geoenvironmental Engineering*, vol. 131, no. 11, pp. 1399–1410, 2005.

[10] V. Avgerinos, D. Potts, and J. Standing, "Numerical investigation of the effects of tunnelling on existing tunnels," *Geotechnique*, vol. 69, pp. 808–822, 2017.

[11] J.-I. Choi and S.-W. Lee, "Influence of existing tunnel on mechanical behavior of new tunnel," *Ksce Journal of Civil Engineering*, vol. 14, no. 5, pp. 773–783, 2010.

[12] P. Li, S.-J. Du, S.-L. Shen, Y.-H. Wang, and H.-H. Zhao, "Timoshenko beam solution for the response of existing tunnels because of tunneling underneath," *International Journal for Numerical and Analytical Methods in Geomechanics*, vol. 40, no. 5, pp. 766–784, 2016.

[13] H. M. Shahin, T. Nakai, K. Ishii, T. Iwata, and S. Kuroi, "Investigation of influence of tunneling on existing building and tunnel: model tests and numerical simulations," *Acta Geotechnica*, vol. 11, no. 3, pp. 679–692, 2016.

[14] H.-B. Yun, S.-H. Park, N. Mehdawi et al., "Monitoring for close proximity tunneling effects on an existing tunnel using principal component analysis technique with limited sensor data," *Tunnelling and Underground Space Technology*, vol. 43, pp. 398–412, 2014.

[15] J. Fu, J. Yang, L. Yan, and S. M. Abbas, "An analytical solution for deforming twin-parallel tunnels in an elastic half plane," *International Journal for Numerical and Analytical Methods in Geomechanics*, vol. 39, no. 5, pp. 524–538, 2015.

[16] M.-f. Lei, D.-y. Lin, W.-c. Yang, C.-h. Shi, L.-m. Peng, and J. Huang, "Model test to investigate failure mechanism and loading characteristics of shallow-bias tunnels with small clear distance," *Journal of Central South University*, vol. 23, no. 12, pp. 3312–3321, 2016.

[17] B. Zhang, X. Wang, J.-s. Zhang, J.-h. Zhang, and H. Cheng, "Safe range analysis of clear distance of twin shallow tunnels based on limit analysis and reliability theory," *Journal of Central South University*, vol. 25, no. 1, pp. 196–207, 2018.

[18] Y. Fang and C. He, "Numerical analysis of the influence of parallel shield tunnel construction on existing tunnels," *Geomechanics*, vol. 28, pp. 1402–1406, 2007.

[19] J. Chen, X. Wang, and Z. Shi, "Interaction analysis of shield tunnel construction in short spacing and large diameter highway," *Geotechnical Mechanics*, vol. 31, pp. 242–247, 2010.

[20] P. Lu, H. Jiang, and G. Zheng, "The impact of the adjacent construction of shield tunnels on the built tunnels," *Journal of Beijing University of Technology*, vol. 40, pp. 1121–1127, 2014.

[21] F. Ye, J. Mao, and Y. Liu, "Model test of dynamic pressure arch effect on surrounding rock of weak and fractured tunnel," *China Journal of Highway*, vol. 28, pp. 76–82, 2015.

[22] E. Almeida, A. Negro, M. Matos Fernandes, and A. Cardoso, "Three-dimensional nonlinear analyses of a metro tunnel in sao paulo porous clay, Brazil," *Journal of Geotechnical and Geoenvironmental Engineering*, vol. 137, pp. 376–384, 2011.

[23] J. Kim, H. Rehman, and W. Ali Weightage, "Effect during back-calculation of rock-mass quality from the installed tunnel support in rock-mass rating and tunneling quality index system," *Applied Sciences-Basel.*, vol. 9, 2019.

[24] C. Y. Gue, M. J. Wilcock, and M. M. Alhaddad, "Tunnelling close beneath an existing tunnel in clay - perpendicular undercrossing," *Geotechnique*, vol. 67, pp. 795–807, 2017.
[25] Y. Xiang, *An Introduction to Tunnel Mechanics*, Science Press, Beijing, China, 2014.
[26] Y. Zhang, Z. Yin, and Y. Xu, "Surface deformation analysis caused by shield tunneling," *Journal of Rock Mechanics and Engineering*, vol. 21, pp. 388–392, 2002.
[27] J. Pan, *Analysis of the Influence of Shenzhen Composite Stratum on the Stress and Deformation of Shield Tunnel Lining Segment Structure*, Beijing Jiaotong University, Beijing, China, 2015.